X-ray Structures of a Designed Binding Site in Trypsin Show Metal-Dependent Geometry[†,‡]

Linda S. Brinen,[§] W. Scott Willett,[||,⊥] Charles S. Craik,[||] and Robert J. Fletterick*[,§]

Department of Biochemistry and Biophysics and Department of Pharmaceutical Chemistry, University of California at San Francisco, San Francisco, California 94143

Received December 20, 1995; Revised Manuscript Received March 15, 1996[⊗]

ABSTRACT: The three-dimensional structures of complexes of trypsin N143H, E151H bound to ecotin A86H are determined at 2.0 Å resolution *via* X-ray crystallography in the absence and presence of the transition metals Zn^{2+}, Ni^{2+}, and Cu^{2+}. The binding site for these transition metals was constructed by substitution of key amino acids with histidine at the trypsin−ecotin interface in the S2′/P2′ pocket. Three histidine side chains, two on trypsin at positions 143 and 151 and one on ecotin at position 86, anchor the metals and provide extended catalytic recognition for substrates with His in the P2′ pocket. Comparisons of the three-dimensional structures show the different geometries that result upon the binding of metal in the engineered tridentate site and suggest a structural basis for the kinetics of the metal-regulated catalysis. Of the three metals, the binding of zinc results in the most favorable binding geometry, not dissimilar to those observed in naturally occurring zinc binding proteins.

Metal ions serve to enhance the structural stability of a protein in a conformation that is critical for biological function or take part in the catalytic processes of enzymes (Glusker, 1991). In fact, nearly one-third of all known proteins require metal ions for their structure or function (Ibers & Holm, 1980). There is significant interest, therefore, in further understanding how these metals interact with and confer special properties to metal-containing proteins. As mechanisms of binding and interaction are clearly understood, engineered metal sites may be constructed to tailor protein function, for example, to inhibit protease activity (Halfon & Craik, 1996; Higaki et al., 1990; McGrath et al., 1993), or to activate glycogen breakdown (Browner et al., 1994), or to bind metal to an antibody (Roberts, 1990).

In recent years, a sizable library of structurally characterized metal-containing compounds has amassed. Three-dimensional atomic structural information is currently available in the Cambridge Structural Database (Allen et al., 1979) for more than 50 000 organometallic small molecule compounds, approximately 20% of them containing either zinc, copper, or nickel atoms. At the present time, there are more than 30 structurally characterized naturally occurring zinc-, copper-, and nickel-containing proteins in the Brookhaven Protein Data Bank, including the zinc binding horse liver alcohol dehydrogenase (Schneider et al., 1983) and carboxypeptidase A (Quiocho & Lipscomb, 1971; Rees et al., 1983), nickel-containing urease (Jabri et al., 1995), and type 1 copper binding proteins azurin from *Pseudomonas aeruginosa* (Adman et al., 1978; Adman & Jenson, 1981) and from *Alcaligenes dentrificans* (Norris et al., 1983, 1986), as well as plastocyanin (Guss & Freeman, 1983; Guss et al., 1986). These and other examples (Fuh & Walls, 1995; Hall et al., 1995; He et al., 1995; Regan, 1995; Somers et al., 1994; Yagami-Hiromasa et al., 1995) demonstrate the important roles that metal ions have been found to play in proteins. They also have provided the basis of information from which modeling and engineered systems have been initiated.

Structures of a few *engineered* metal binding proteins have recently emerged. Numerous carbonic anhydrase variants bound to zinc (Ippolito & Christianson, 1994; Lesburg & Christianson, 1995), for example, are representative of naturally occurring metal binding sites that have been modified or "reengineered". The variants trypsin R96H bound to copper (McGrath et al., 1993) and phosphorylase V45H, Y75H bound to nickel (Browner et al., 1994) are the only known X-ray crystal structures of bidentate *de novo* designed protein−metal binding sites. The question of whether or not a *de novo* engineered *tri*dentate site that modified enzyme function could be accomplished within allowable protein geometry constraints was then raised. Could the availability of flexible loop regions be employed for strategic binding site design? A tridentate site might be more specific and possibly more stable, depending on the resulting structural ramifications of the engineered protein.

Rat anionic trypsin functions well as a model system to test the design of metal binding sites since it has an established expression and purification system, well-defined assays for kinetic analysis, and a long history of successful crystallization and strong diffraction. Alteration of substrate specificity to include recognition of histidine has been engineered previously into trypsin by creating binding sites for Ni^{2+} and Zn^{2+} ions (Willett et al., 1995). This was achieved by creating a tridentate site involving amino acid residues 143 and 151 of trypsin along with the P2′ site of

[†] This work supported in part by NIH Grant DK39304-06A2 to R.J.F. and NSF Grant MCB-9219806 to C.S.C. L.S.B. is supported by the Program of Excellence in Molecular Biology at the University of California, San Francisco. W.S.W. is supported by the University of California Biotechnology Research and Education Program.

[‡] Atomic coordinates have been deposited with the Brookhaven Protein Data Bank, file names 1SLU, 1SLV, 1SLW, and 1SLX for the apo, copper-bound, nickel-bound, and zinc-bound structures, respectively (Bernstein et al., 1977).

* To whom correspondence should be addressed.

[§] Department of Biochemistry and Biophysics.

[||] Current address: Department of Chemistry and Biochemistry, University of Colorado at Boulder, Boulder, CO 80303.

[⊥] Department of Pharmaceutical Chemistry.

[⊗] Abstract published in *Advance ACS Abstracts,* April 15, 1996.

S0006-2960(95)03020-0 CCC: $12.00

the substrate ecotin. The use of histidine side chains in conjunction with zinc, copper, and nickel was selected because histidines have the ability to readily donate a lone pair of electrons to these transition metals. The coordination bonds formed between the imidazole nitrogen and metal are both stable and reversible. Furthermore, in an aqueous environment, the bonds formed by zinc, copper, and nickel will be preferential for imidazole nitrogens as opposed to the acetate groups favored by calcium and magnesium.

The accompanying paper (Willett et al., 1996) to this work described the rationale, modeling, and kinetic characterization of this engineered trypsin−ecotin complex in the absence and presence of Zn^{2+}, Ni^{2+}, and Cu^{2+}, and the kinetic results raise an interesting question. The activating potential of the three metal ions was found to be the inverse of that predicted solely on the basis of chemical affinity of the metals for free imidazole in solution (Martell & Smith, 1974; Higaki et al., 1990). While some hypotheses can be made to explain the observed kinetic effect, additional information can be gleaned by examining the local and global conformational details of the metal-regulated engineered complexes, visible only *via* three-dimensional structure elucidation. This paper describes the X-ray crystallographic structure determination of the engineered trypsin N143H, E151H bound to the engineered substrate ecotin A86H in the absence and presence of three different transition metals. Extensive studies that serially mutate amino acid residues in the vicinity of a particular binding site have been done before, but this work represents the first successful X-ray crystallographic investigation of a *de novo* engineered tridentate metal binding site in the absence and presence of a series of metal ions. Not only do these structures demonstrate that prediction and design based on the information amassed from known metal binding sites are still an imperfect science but they provide the basis for interpretation of the kinetic effect just described. Upon comparison of the environments of the three different metals in the trypsin−ecotin complexes, the smallest perturbations from the expected structure were found in the case of zinc binding. This suggests that proper catalytic register is preserved, accounting for the observed kinetics result in the presence of zinc.

EXPERIMENTAL PROCEDURES

Crystallization and Metal Soaks. The preparation and purification of trypsin N143H, E151H (subsequently referred to as Tn N143H, E151H) has been described previously (Willett et al., 1995), and the preparation and purification of ecotin A86H (subsequently referred to as Ec A86H) was described in the accompanying paper. Tn N143H, E151H which had been concentrated to ∼1 mM in 1 mM HCl, pH 3.0, was mixed with Ec A86H in equimolar amounts in a 0.5 mL eppendorf tube on ice. To this mixture were added 3 M NaOAc and 1 M Tris, pH 8.0, such that the final concentrations were as follows: trypsin and ecotin, 375 μM; NaOAc, 300 mM; and Tris, 100 mM. The resulting pH of this solution was 8.0. The trypsin−ecotin complex was crystallized using the hanging drop method (McPherson, 1989) over a well solution of 18−22% PEG 4000 (Alltech)/300 mM NaOAc/100 mM Tris, pH 8.0/10 mM $CaCl_2$. Drops containing a mixture of 2 μL of protein solution and 2 μL of well solution typically produced elongated prism-shaped crystals after 2−3 days at 18 °C. Crystals intended for soaking in metal solutions were stabilized in an artificial mother liquor of 25% PEG 4000/300 mM NaOAc/10 mM Tris, pH 8.0, before being soaked in increasing amounts of either copper-, nickel-, or zinc-laden artificial mother liquor. A typical metal soaking procedure involved successive soaks in artificial mother liquor solutions of 1 μM, 10 μM, 100 μM, and finally 1 mM metal concentration, with soaking times at each concentration ranging from 30 min to 18 h. In an attempt to remove free and nonspecifically bound metal from solvent channels, the metal-soaked crystals were briefly back-soaked in metal-free artificial mother liquor prior to data collection.

Data Collection and Reduction. All X-ray diffraction data were measured at room temperature on an R-axis IIc imaging plate with a Rigaku RU-200 rotating anode generator operating at 15 kW (50 mA and 300 kV) with graphite monochromated Cu Kα radiation ($\lambda = 1.5418$ Å). Exposure times were constant throughout each individual data set and were either 15 or 20 min/deg, depending on the intensity of the diffraction of the crystal. While numerous crystals were tested for diffraction and several complete data sets were measured for both the apo crystals and for complexes with each of the metals in question, each structure was ultimately solved on the basis of data obtained from one single crystal. All diffraction data were indexed, integrated, scaled, and merged with the HKL software package (Otwinowski, 1990).

Parameterization of Metals for Structure Refinement. The parameters used to describe and restrain the copper ion in its interactions with the histidine side chains were derived as described by McGrath et al. (1993). The values are based on a combination of van der Waals and electrostatic terms, as well as bond and angle connectivity information, the latter being obtained from seven known copper binding proteins found in the Brookhaven Protein Data Bank. Since there is no comparable data base of zinc or nickel binding proteins from which to derive *ab initio* force fields, slight generalizations were made to the copper parameter set to allow for its application to the zinc- and nickel-containing structures. Harmonic force constants were selected such that a displacement from the reference value equal to twice the standard deviation ($\sigma = 0.5$ Å for bonds, $\sigma = 10°$ for angles) would require 1.0 kcal/mol for bonds and 0.5 kcal/mol for angles, and the charge of each metal was set to +2. The primary concern in establishing these force fields was that the ultimate geometry around each metal center not be biased by the input starting values of the positional or restraint parameters. To address this concern, the weighting scheme applied to geometric constraints was consistently kept very loose during refinements with X-PLOR, allowing the observed geometries to be dictated predominantly by the experimental data. It was found that imposing these weak restraints, particularly in the early stages of refinement, assured a reasonable starting geometry for the metal binding sites.

RESULTS

Crystallographic Results. A summary of the data collection and processing statistics can be found in Table 1. All

[1] Abbreviations: Tn N143H, E151H, trypsin N143H, E151H; Ec A86H, ecotin A86H; $Tn^{‡}E^{†}$, complex of Tn N143H, E151H with Ec A86H; $Tn^{‡}E^{†}Zn$, complex of Tn N143H, E151H with Ec A86H and zinc; $Tn^{‡}E^{†}Cu$, complex of Tn N143H, E151H with Ec A86H and copper; $Tn^{‡}E^{†}Ni$, complex of Tn N143H, E151H with Ec A86H and nickel.

Table 1: Data Collection and Reduction Statistics for Tn‡E†, Apo and Complexes

structure	Tn‡E†Apo	Tn‡E†Zn	Tn‡E†Cu	Tn‡E†Ni
final metal concn (mM)		1.0	0.1	1.0
total soak time (h)		18	4−6	18
unit cell				
a (Å)	85.15	85.98	86.35	86.38
b (Å)	56.18	56.28	56.59	56.23
c (Å)	80.68	81.86	81.40	81.23
β (deg)	91.75	92.18°	92.99	92.81
max resolution (Å)	1.8	2.2	2.3	2.0
total observations	86638	46301	58971	56521
unique observations[a]	19067 (2*σ*)	10021 (1.5*σ*)	16190 (1.5*σ*)	17281 (1.5*σ*)
completeness (%)	98.4	90.9	96.1	95.5
high-resolution shell (%)	94.3	87.4	92.7	90.4
R_{merge} (%)[b]	4.6	6.5	6.4	5.4

[a] Reflections used in structure refinement at *σ* level indicated. [b] $R_{merge} = \sum|(I - \langle I\rangle)|/\sum(I)$.

four structures described belong to the monoclinic space group *C*2 and have one molecule of Tn N143H, E151H bound to one molecule of Ec A86H in the asymmetric unit, though the unit cell parameters varied by as much as 1.5% between the different soaks and the apo crystals. (The complex of Tn N143H, E151H with Ec A86H will subsequently be referred to as Tn‡E†.) Since crystals of the Tn‡E† complex typically grew in polycrystalline clusters, finding a crystal containing one unique lattice was challenging and required the screening of numerous crystal samples. The quality and diffracting power of single crystals, however, were quite good for all cases, although the apo crystals were significantly more resilient to decay than were the metal-soaked crystals. As a result, data from the last hours of measurement that indicated greater than 20% dropoff in diffraction intensity at highest resolution were not used in the structure refinement process. Since this is not an optimal solution to the decay problem, the possibility of conducting data collection at liquid nitrogen temperatures was explored. This was not a viable option, however, since crystals of Tn‡E† were prone to fissuring and fracturing, a condition only aggravated upon freezing. Furthermore, prolonged exposure to metal ion solution noticeably weakened the physical integrity of the crystals, particularly in the case of the copper soak. As a result of this sensitivity, the copper soak had to be shortened to 6 h in a 10-fold less concentrated metal solution than either the nickel or zinc in order to avoid complete crystal decomposition upon subsequent crystal handling. Cocrystallization of the complex of Tn‡E† with each metal was attempted as an alternative to soaking the apo samples; however, this approach did not yield any crystals.

Structure Solution and Refinement. All four structures were solved *via* the molecular replacement method. The apo structure was solved with the conventional rotation and translation functions of the X-PLOR package (Brunger et al., 1987), using one monomer of the space group $P2_1$ trypsin−ecotin dimer complex structure as a search model (McGrath et al., 1994). All waters were excluded from the search model. The three metal-containing structures were solved with either X-PLOR or AMoRe (Navaza, 1994), using the fully refined Tn‡E† apo structure, again without waters, as a search model. Details pertaining to structure solution and refinement for all four structures can be found in Table 2. It is surprising to note that molecular replacement was necessary in order to correctly place the apo model into the experimental data for each of the metal-containing crystals. It was expected that the fully refined apo structure of Tn‡E† could be used directly as a starting model for refinement of the metal-containing structures. However, when this strategy was used, the refinement process routinely stalled, as reflected by the crystallographic *R*-factor staying above 24%, a value that appeared to be too high considering the quality of the data, the starting model in use, and the electron density maps under consideration. Standard rotation and translation searches were completed, and the resulting placement of the molecule was compared to the placement of the molecule with the suspiciously high *R*-factor. The orientation of the two differed by greater than 2°. Apparently, the radius of convergence of standard X-PLOR rigid-body refinement had not been large enough to accommodate the nonisomorphism of these samples with respect to one another. Once the correct rotation angles were applied and positional and *B*-factor refinement continued, the crystallographic *R*-factor consistently dropped below 20%.

Table 2: Structure Solution and Refinement Statistics for Tn‡E†

structure	Tn‡E†Apo	Tn‡E†Zn	Tn‡E†Cu	Tn‡E†Ni
R after molec repl (%)[a]	45.2	35.1	34.5	37.8
resolution range (Å)	5.0−1.8	6.0−2.2	6.0−2.3	6.0−2.0
R[a]	19.5	17.3	19.5	17.9
free *R*[b]	28.5	26.7	27.8	25.3
putative water molecules	137	64	67	53
metal occupancy (%)		100	84	99
⟨bonds⟩ (Å)	0.005	0.005	0.006	0.006
⟨angles⟩ (deg)	1.2	1.1	1.2	1.3
average *B* (trypsin)	29.8	24.1	32.2	38.3
average *B* (ecotin)	36.2	33.8	40.2	44.9

[a] $R = \sum_{h,k,l}(|F_o(h,k,l)| - k|F_c(h,k,l)|)^2$. [b] Cross-validation *R* calculated by omitting 10% of reflections to serve as a statistical test (Brunger et al., 1987).

Electron density display, model building, and modification were performed with the program CHAIN (Sack, 1988). Fourier syntheses, using coefficients of $3F_o - 2F_c$, $2F_o - F_c$, and $F_o - F_c$, were routinely inspected after each round of positional and *B*-factor refinement so that appropriate changes to main and side chains could be made in the model where indicated. In all four structures, the area requiring the most manual deletion and rebuilding of residues was the trypsin autolysis loop region, residues 144−150. As is common in numerous trypsin crystal structures, some or all of the autolysis loop residues were too disordered to be observed in electron density maps of three of the Tn‡E† structures. Only in the zinc-containing structure is this loop fully ordered and visible. In sharp contrast, initial difference electron density syntheses ($F_o - F_c$) using all data between 15 and 3.0 Å showed unambiguous density for each of the metal ions. For the zinc-soaked crystals, the difference density peak was observable at better than 6*σ*; for nickel, 7*σ*; and for copper, better than 5*σ*. The percent occupancy of each metal was refined using X-PLOR and revealed that the zinc site was 100% occupied, the nickel site 99% occupied, and the copper site 84% occupied. The refined *B*-factor of each of the metals was normal and consistent with the *B*-values of the surrounding residues. Water molecules were added manually to all three structures according to the criteria of good electron density (at least

3.5σ in difference maps) as well as acceptable hydrogen bond distance and geometry to adjacent atoms.

The region of trypsin residues 113−117 was consistently unobserved in the electron density maps of all four Tn‡E† structures solved. SDS−PAGE and N-terminal sequencing analysis described in the previous paper suggests that an autolysis product was generated during the crystallization process. Autolysis at Arg 117, as well as cleavage that could have taken place at the lysine at position 113, presumably accounts for the lack of electron density for the segment between 113 and 117. The consistent presence of a water molecule in the vicinity of this cleavage point further supports this explanation. Ecotin residues 90 and 91 were consistently disordered and not visible in any of the four structures considered in this study. This region showed similar disorder in the $P2_1$ structure of trypsin−ecotin (McGrath et al., 1994).

Metal Binding Centers. Figure 1 illustrates the electron density observed in the local area of Tn‡E†. This figure clearly shows that each metal is in fact bound with well-ordered occupancy (100%, 84%, and 99% occupancy for Zn, Cu, and Ni, respectively) to the engineered tridentate site and that, in contrast, there is no density present between the three imidazole rings in the apo structure. Furthermore, there is no evidence of any other fully or partially occupied metal binding sites in the trypsin−ecotin complex, although copper and silver have been observed to bind to His 57 in trypsin at higher concentrations of metal (Chambers et al., 1974). It should be noted, however, that the electon density observed for His 151 in all four structures is less satisfactory than the density observed for the other engineered histidines. The *B*-factors for His 151 range from 50 to 61 (averaged over all atoms), which is significantly higher than the *B*-factors observed for His 86 and His 143. While the position of the main chains in this region are roughly superimposable, there are significant differences in the position and orientation of the side chains dependent upon the presence and type of metal. There are also other notable differences in the local structure. In both the nickel- and copper-bound structures, there is an ordered visible water molecule occupying one of the metal coordination sites. In the zinc structure, however, there is no visible water molecule occupying the fourth coordination site. While it is possible that a loosely bound water exists in solution, any water molecule present is too disordered to see at 2.2 Å resolution in electron density maps calculated from data measured at room temperature. Examination of a space-filling model of the zinc binding site area confirms that there would be adequate room for a water molecule to fill the fourth coordination site. As previously mentioned, the nearby autolysis loop is ordered and visible only in the zinc-bound structure. In both the nickel and copper structures, residues 146−149 are disordered and are therefore not observed.

Figure 2 is a schematic representation of the metal centers in the three metal-bound structures of Tn‡E†. The details of the local geometries of each metal binding site are summarized in Table 3. All bonds between metal and the histidine side chain are made to the ϵ-nitrogen of the imidazole ring. While none of the sites can be simply described as any one geometry, the zinc site resembles a distorted tetrahedral arrangement with bond angles of 93.2°, 106.0°, and 100.5° about the metal center. The copper metal center can be described as a distorted square-planar geometry with the Ec A86H (P2′) Nϵ2 on the opposite corner from the Tn N143H Nϵ2 (146.3°) and the water on the opposite corner from Tn E151H Nϵ2 (132.3°). The nickel ligand geometry is neither tetrahedral nor square planar but appears to be based on a square pyramidal arrangement, with the nickel ion occupying the center of the base of the pyramid. The planarity of the metal ions with the imidazole rings is an indication of the quality of the coordinate bond, as metal ions tend to bind in the plane of the ring along the direction of the nitrogen lone pair (Chakrabarti, 1990). In the structures described, the deviation from planarity of the metal ion with respect to the imidazole ring of the histidine is described by the perpendicular distance of the metal ion from the plane defined by the atoms of the imidazole ring. The arrangement of the imidazole rings about the zinc is the closest to coplanar, with deviations of 0.22, 0.44, and 0.07 Å. The arrangement about nickel is next best (0.26, 1.24, 0.3 Å), while that of copper shows the greatest total deviation from planarity (1.43, 0.23, 0.66 Å). In fact, visual inspection of the orientation of the imidazole ring of His 86 of ecotin with respect to the copper ion reveals that the interaction of the electron spheres of these two atoms is not favorable although this orientation is indeed representative of the observed electron density in this region. It is interesting to note that no other potential rotomer (Ponder & Richards, 1987) for this residue would result in a better configuration for successful bonding to the metal. In order for a statistically probable conformation of His 86 of ecotin to fit the observed density, a shift on the order of ∼1.5 Å would be necessary in the adjacent main chain atoms. This is not possible with the nearby constraints of a disulfide linkage between Cys 87 and Cys 50 of ecotin.

In the absence of metal ion in the Tn‡E† complex, the histidines comprising the engineered metal binding site are not in conformations that would bind a metal. However, in the presence of zinc, copper, or nickel, all three histidines form a metal binding site that resembles the model described and illustrated in the accompanying paper. The conformational changes—in the side chains as well as the corresponding main chain atoms—that occur in the local environment of the engineered histidine pocket upon introduction of zinc are illustrated in superposition against the apo pocket in Figure 3. The local environments of the three metal binding sites are shown in superposition with one another in Figure 4. The changes observed in these figures are summarized as root mean square deviations in Table 4. In order to calculate the root mean square deviations reported, two different superposition experiments were done. First, only the three histidine side chains were superimposed, and their root mean square deviations were calculated, reported in boldface type. Second, all main chain atoms in an approximately 15 Å radius of the metal binding site were superimposed, and the resulting root mean square deviations are reported in italics.

Hydrogen-Bonding Networks. In the absence of metal ion, the conformations of the engineered histidine residues are readily visible in the experimentally determined electron density maps. The hydrogen-bonding pattern of the three histidine residues serves to stabilize the positions of the imidazole rings to some extent. The conformations of two of the three histidines correspond to the statistically most probable rotomer (Ponder & Richards, 1987), the rotomer choice for His 143 of trypsin being the exception. The

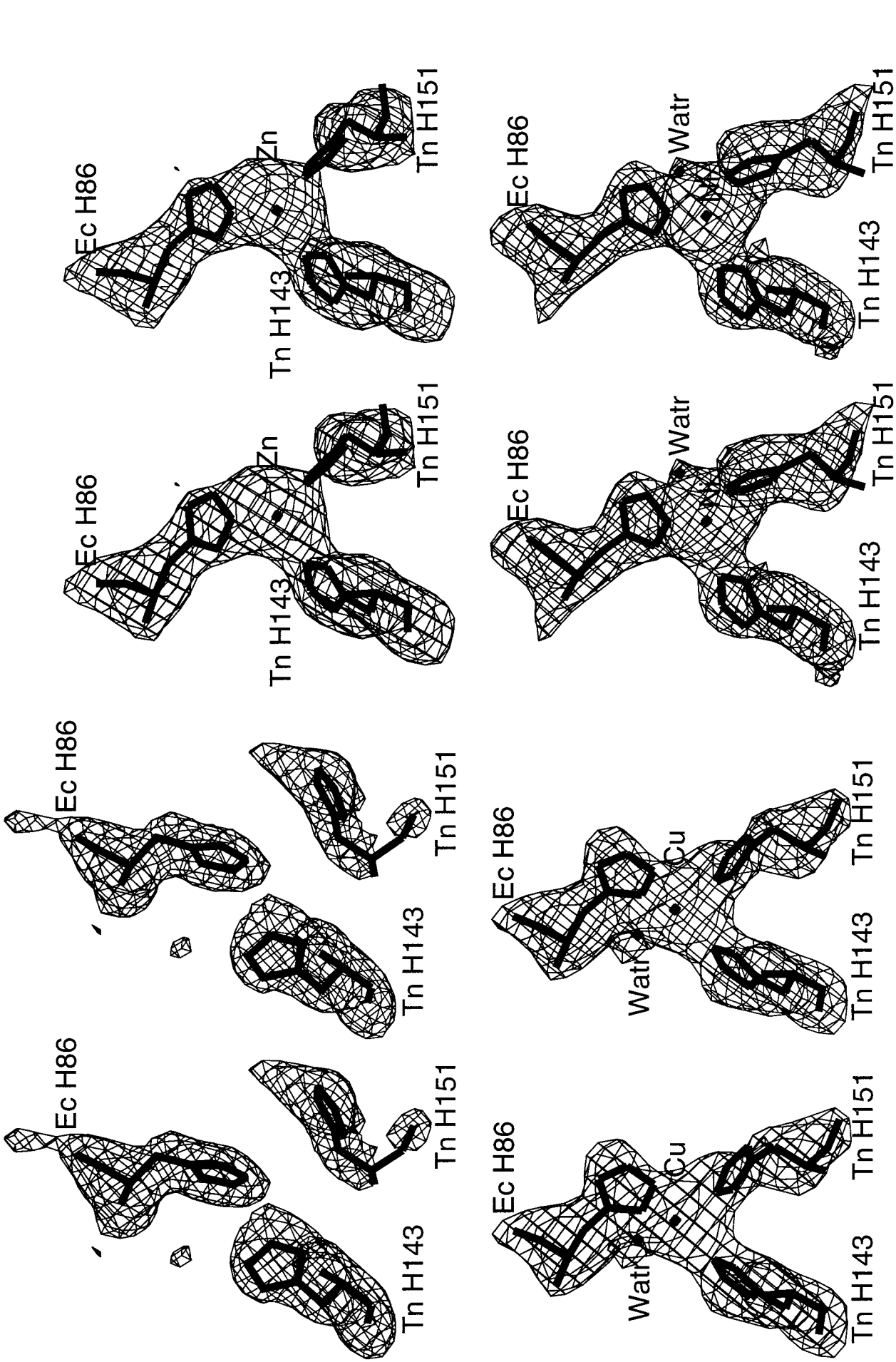

FIGURE 1: Stereoviews of electron density (simulated annealing omit maps contoured at 2.5σ) in the engineered metal binding pocket. Density is displayed with CHAIN. Tn N143H, E151H and Ec A86H are indicated, as are metals, where present. (a, top left) Tn‡E†, (b, top right) Tn‡E†Zn, (c, bottom left) Tn‡E†Cu, and (d, bottom right) Tn‡E†Ni.

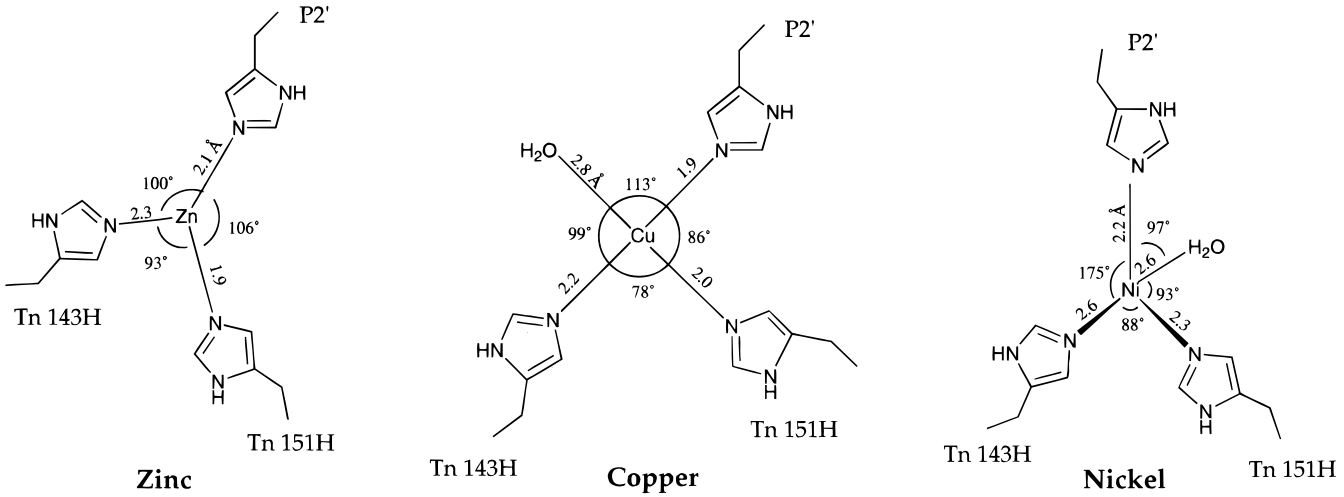

FIGURE 2: Schematic representation of metal coordination geometry in Tn‡E†Zn, Tn‡E†Cu, andTn‡E†Ni.

Table 3: Metal Center Geometries of Tn‡E† Complex Structures

	Tn‡E†Zn	Tn‡E†Cu	Tn‡E†Ni
distances (Å)[a]			
Ec 86H (P2′) His Nϵ2−M^{2+}	2.12	1.87	2.15
Tn 143 His Nϵ2−M^{2+}	2.32	2.18	2.61
Tn 151 His Nϵ2−M^{2+}	1.91	1.97	2.26
H_2O−M^{2+}		2.78	2.60
angles (deg)[b]			
Tn 143−M^{2+}−Tn 151	93.17	78.50	87.72
Tn 143−M^{2+}−Ec 86 (P2′)	100.51	146.30	77.71
Tn 151−M^{2+}−Ec 86 (P2′)	106.05	85.77	86.37
Tn 143−M^{2+}−H_2O		99.17	174.97
Tn 151−M^{2+}−H_2O		132.33	93.10
Ec 86 (P2′)−M^{2+}−H_2O		113.29	97.38
metal−imidazole nonplanarity (Å)[c]			
Ec 86 (P2′) His	0.22	1.43	0.26
Tn 143 His	0.44	0.23	1.24
Tn151 His	0.07	0.66	0.30

[a] Distances are measured between the Nϵ2 atom of the indicated histidine residue and metal ion (M^{2+}). [b] Angles are measured between the Nϵ2 atoms of the indicated histidine residue and the metal ion. [c] The nonplanarity of the metal ion is measured as the perpendicular distance of the metal out of the plane defined by the imidazole ring.

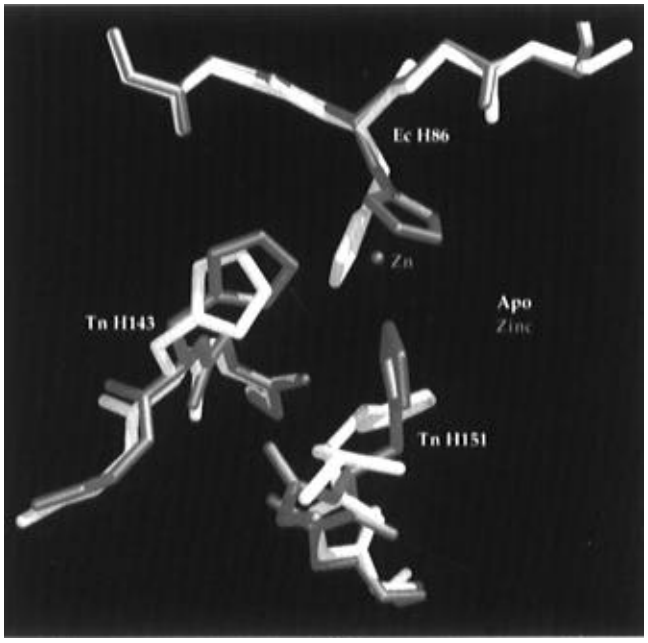

FIGURE 3: Superposition (based of Cα of trypsin, immediate vicinity of metal binding region excluded) of the engineered metal binding pocket of the Tn‡E†Zn structure on the apo Tn‡E† structure. The root mean square deviation for superposition of these two structures in this region is 1.49 Å. Figure prepared with MidasPlus.

position of His 143 is determined by two interactions on the part of the Nδ1 atom of His 143. First, there is a 3.1 Å hydrogen bond with the Oϵ1 atom of Tn 192 (Gln), and second is a longer 3.3 Å weak polar interaction with the backbone carbonyl oxygen of Tn 192. The Nϵ2 atom of His 151 donates a hydrogen bond to the backbone carbonyl oxygen of Tn 141 (Trp) 3.2 Å away, and it also is involved in a weak polar interaction with the backbone carbonyl oxygen of Tn 152 (Pro) 2.8 Å away. The P2′ residue Ec A86H is involved in one potential weak polar interaction with an ordered water 2.8 Å from the Nδ1 atom of the imidazole ring.

In the metal-bound structures, the local geometry and hydrogen-bonding patterns are markedly different. In all cases, the P2′ histidine and His 151 have swung around into position to bind the metal, which is reflected by large changes in the χ_1 angles of these residues. The changes observed in the orientation of His 143 are less dramatic and are mostly reflected in changes in χ_2. All values of χ_1 and χ_2 for the apo and metal-bound structures are found in Table 5. [It is interesting to note the contrasts between the conformational changes induced by metal binding in this three-histidine site and the lack of conformational changes accompanying the binding of metal to the three-histidine site of apocarbonic anhydrase II; see Håkansson et al. (1992).]

In each metal-bound structure, the Nϵ2 atoms of His 143, His 151, and His 86 are all coordinated to the metal. In the zinc structure, the Nδ1 atom of the P2′ residue donates a hydrogen to the carbonyl oxygen of Tn 40 (His). The Nδ1 atom of His 151 also interacts with a main chain atom, making a 2.7 Å polar interaction to the carbonyl oxygen of Tn 149 (Val). The Nδ1 atom of His 143 continues to be weakly associated with the Oϵ1 of Tn 192 (Asn) at a distance of 3.5 Å. In the copper structure, the Nϵ2 atom of the P2′ residue forms a possible weak polar interaction with a water molecule 3.5 Å away. The Nδ1 atom of this residue is involved in a 3.4 Å polar interaction with the backbone atom carbonyl oxygen of Ec 87 (Cys). In the nickel-bound structure, the P2′ Nδ1 atom also interacts with the carbonyl oxygen of Ec 87 3.2 Å away. A weak 3.3 Å hydrogen bond

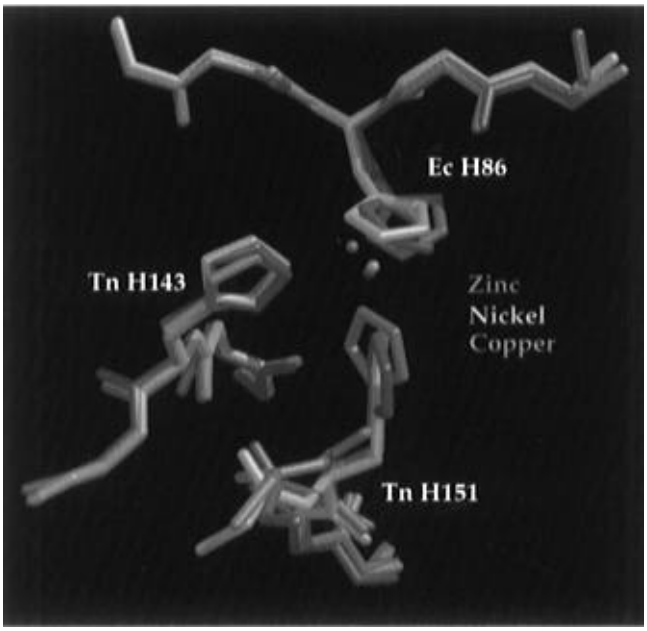

FIGURE 4: Superposition (based on Cα of trypsin, immediate vicinity of metal binding region excluded) of the engineered metal binding pocket and metals for the $Tn^{‡}E^{†}Zn$, $Tn^{‡}E^{†}Cu$, and $Tn^{‡}E^{†}$-Ni structures. The root mean square deviations for superposition of the metal structures against $Tn^{‡}E^{†}$ are 1.49, 1.33, and 1.61 Å, respectively. The three metal-bound loop regions show more similarity to one another than any of them shows to $Tn^{‡}E^{†}$. Figure prepared with MidasPlus.

Table 4: Main Chain and Side Chain Superposition in the Engineered Metal Binding Site[a]

	$Tn^{‡}E^{†}$	$Tn^{‡}E^{†}Zn$	$Tn^{‡}E^{†}Cu$	$Tn^{‡}E^{†}Ni$
$Tn^{‡}E^{†}$		0.71	0.63	0.82
$Tn^{‡}E^{†}Zn$	**3.3**		0.49	0.47
$Tn^{‡}E^{†}Cu$	**3.3**	**0.63**		0.38
$Tn^{‡}E^{†}Ni$	**3.3**	**0.84**	**0.87**	

[a] Boldface, superposition of Tn 143H, 151H, Ec 86H side chains only; italics, superposition of surrounding main chain atoms. Values given for ⟨rms⟩ deviation are in angstroms.

Table 5: Values of χ_1 and χ_2 for Ec 86H, Tn 143H, and Tn 151H[a]

	$Tn^{‡}E^{†}$	$Tn^{‡}E^{†}Zn$	$Tn^{‡}E^{†}Cu$	$Tn^{‡}E^{†}Ni$
Ec 86H (P2′) χ_1	−98.5	−155.5	−156.9	−159.3
Ec 86H (P2′) χ_2	−49.4	−135.1	−84.2	−98.4
Tn 143H χ_1	−70.3	−64.4	−60.6	−63.2
Tn 143H χ_2	120.3	172.4	−170.1	170.7
Tn 151H χ_1	170.6	−71.3	−52.9	−106.4
Tn 151H χ_2	−151.6	91.0	105.2	−82.0

[a] All values given are in degrees.

is made by His 151, from Nδ1 to a neighboring water molecule. The hydrogen-bonding and weak polar interactions described are illustrated in Figure 5.

Quaternary Structure. Trypsin bound to ecotin forms a heterotetramer composed of two molecules of trypsin plus two molecules of ecotin. The effects of metal binding on the relative positions of the ecotin molecules within the E_2-T_2 tetramer (ET forms the asymmetric unit) were examined by treating each ecotin molecule in an E_2-T_2 heterotetramer as an ellipsoid and measuring the distance between the centers of mass of the two ellipsoids (Browner et al., 1991). The distance measured for apo $Tn^{‡}E^{†}$, $Tn^{‡}E^{†}Cu$, and $Tn^{‡}E^{†}$-Ni was 25.7 ± 0.2 Å, while the largest change was in the case of $Tn^{‡}E^{†}Zn$, where the distance between the centers of mass of the two ecotins was 26.2 Å. This is the same as was found in the $P2_1$ structure of trypsin bound to ecotin, so the changes observed upon metal binding are not considered to be significant. They are on the same order of magnitude as the change incurred by a change of crystal lattice and are representative of ecotin's inherent flexibility.

The relative positioning of ecotin with respect to trypsin in the E_1-T_1 protein complex changes upon complexation with metal. The extent and nature of the changes are dependent upon the specific metal used. If both Tn N143H, E151H and Ec A86H are taken as ellipsoids, they can each be described by a set of three principal axes, and the relative angles between the two ellipsoids can then be calculated. The differences in angles between pairs of principal axes were, in all cases, less than 1.6°, though the orientation of the changes varied. The smallest rotation of Tn N143H, E151H relative to Ec A86H, compared to the orientations of these protein molecules in the apo $Tn^{‡}E^{†}$ structure, is found in the zinc-bound case. Both the nickel- and copper-bound complexes show substantially more rotation, as well as larger deviations in the separation of the centers of mass of trypsin and ecotin when compared to the apo system. The distance between the centers of mass of trypsin and ecotin changed the most (0.19 Å) in the case of the nickel structure with respect to the distance observed in the apo structure and the least in the case of the zinc structure (0.13 Å).

DISCUSSION

Choice of Substrate. The pan-specific protease inhibitor, ecotin, was selected as the model for bound substrate for Tn N143H, E151H for a number of reasons. First, ecotin's convenient recombinant expression system allowed for the preparation and purification of reagent quantities of a variant possessing a histidine at the P2′ position. Furthermore, the three-dimensional structure of the trypsin−ecotin complex in space group $P2_1$ (McGrath et al., 1994) clearly indicated that, while ecotin is technically an inhibitor, the interactions between the two molecules closely mimicked that of enzyme and substrate. The broad specificity of the inhibitor and the multistrand superstructure of ecotin suggested that ecotin would facilitate the completion of the tridentate metal binding model.

Crystallization and the Crystal Lattice. It is interesting to note that the complex of $Tn^{‡}E^{†}$ did not crystallize under the same conditions as the space group $P2_1$ trypsin−ecotin complex. The space group $P2_1$ crystals contained two molecules of the trypsin−ecotin complex (one heterotetramer, referred to as E_2-T_2) per asymmetric unit. The structures described in this study exhibit similar quaternary structure, packing two ecotin and two trypsin molecules into an E_2-T_2 heterotetramer. However, an additional symmetry constraint is satisfied by the engineered triple variant complex which crystallizes in the centered monoclinic space group *C*2. The crystallographic 2-fold symmetry operator sits adjacent to the autolysis loop region of trypsin, proximal to the three engineered histidine residues involved in metal binding. Presumably, the histidine engineering in an area that is prone to disorder and flexibility in trypsin leads to an increase in crystallographic symmetry.

Individual *B*-factors for particular atoms are indicative of an atom's vibration or disorder. The overall average *B*-factor of each structure is indicative of more global features of the

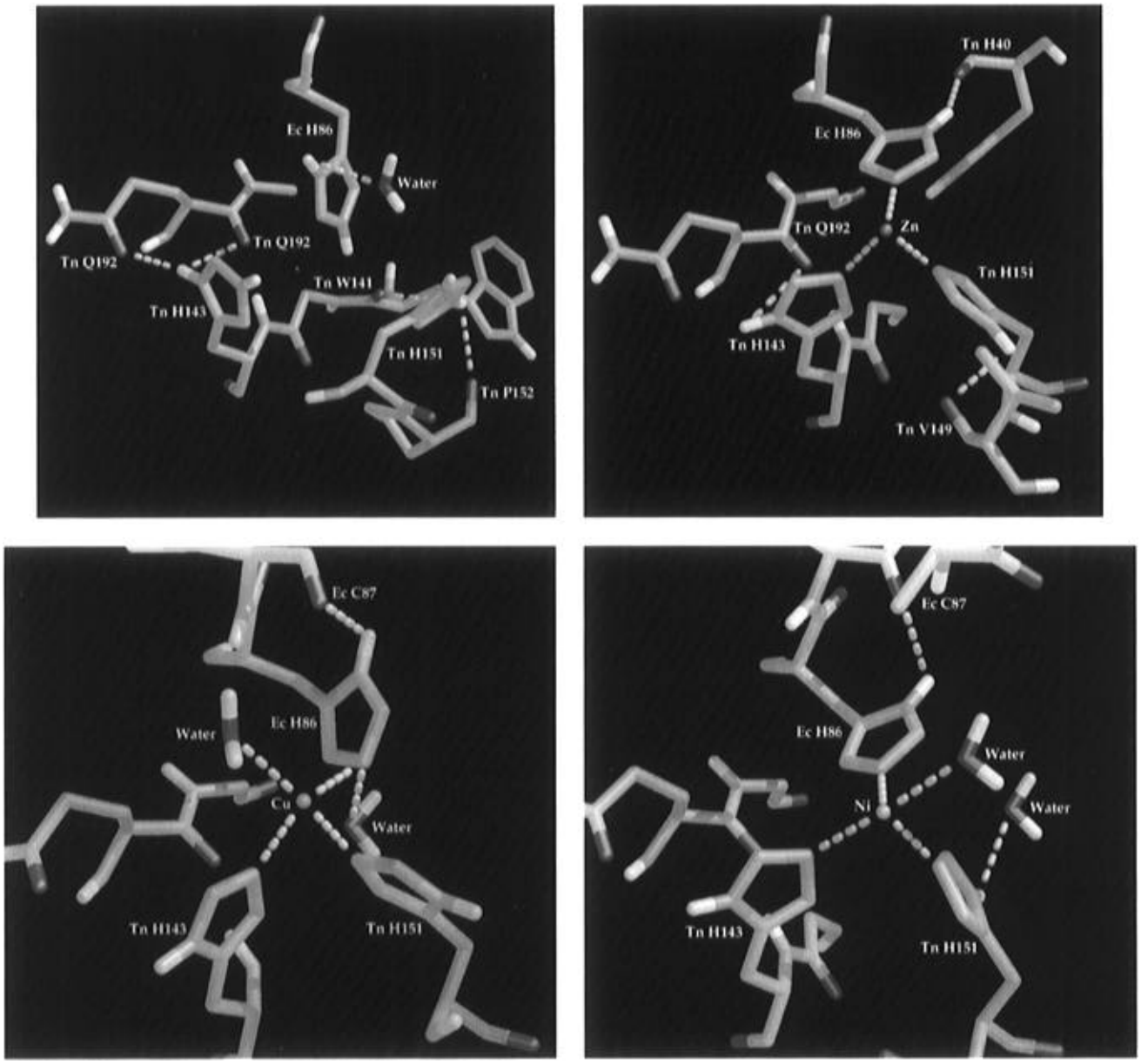

FIGURE 5: Hydrogen-bonding and weak polar interactions in the region of Tn N143H, E151H and Ec A86H: (a, top left) $Tn^{‡}E^{†}$, (b, top right) $Tn^{‡}E^{†}Zn$, (c, bottom left) $Tn^{‡}E^{†}Cu$, and (d, bottom right) $Tn^{‡}E^{†}Ni$. Figures prepared with MidasPlus.

crystal lattice. A general disruption of crystal lattice packing is reflected by an increased average *B*-factor for a structure. The average *B*-values for the various Tn N143H/E151H and Ec A86H in the apo and metal complex structures are higher than would have been predicted on the basis of the quality of each data set, the quality of observed electron density maps, and the resulting refinement statistics (Table 2). However, if the physical integrity of the crystals is considered, the elevated average *B*-factors are understandable. The apo crystals of $Tn^{‡}E^{†}$ were quite prone to fissuring and fracturing. Multiple stress lines were observable in the crystals under magnification with polarized light. These features translated directly into slight packing irregularities in the crystal lattice, as reflected by a significant degree of crystal mosaicity as well as the elevated average *B*-factors for the molecules. Upon the introduction of metals *via* soaking, the potential for disruption of the crystal lattice is enhanced. Predictably, the average *B*-factors for the $Tn^{‡}E^{†}$-Cu and $Tn^{‡}E^{†}Ni$ complexed structures are higher than those of the apo $Tn^{‡}E^{†}$. The average *B*-factor of $Tn^{‡}E^{†}Zn$, however, is lower than that of apo $Tn^{‡}E^{†}$. This can be explained in part by the fact that this structure was refined at lower resolution than the other structures. In addition, the presence of zinc ions appears to have tethered this structure into a higher degree of lattice order, as evidenced by its traceable autolysis loop.

Comparison of Structures. The designed histidine pocket area of the apo and the three metal-bound structures (Figures 3 and 4) shows that, upon binding to metal, the engineered histidine side chains cluster, adopting conformations that assemble the metal binding residues into a roughly similar constellation for coordination to metal. Each of the three metal-bound structures resembles each of the other two metal-bound structures more closely than any one of them resembles the apo nonliganded binding structure in the area of the engineered histidine pocket. There is a consistent trend in all four structures, however. When the crystallographic *B*-factors of each histidine side chain are examined, it is observed that the *B*-factors of His 151 of trypsin are uniformly substantially higher than those of either His 143

of trypsin or His 86 of ecotin, in spite of the fact that His 143 of trypsin appears to be less tightly packed and more solvent-accessible than His 151. Since crystallographic *B*-factors are a measure of atomic vibration or disorder, the magnitudes of which are dependent upon temperature, weight of the atom, and the firmness with which it is held in place by covalent bonds or other forces, it is reasonable to use them to assess the relative level of success achieved in the design of a stable, favorable binding pocket for metal and substrate. On the basis of these criteria, the designed positions of the P2′ histidine and His 143 of trypsin contribute more stability to the engineered site than does His 151 of trypsin. However, there is consistently a bond formed between each metal and the imidazole ring of His 151 of trypsin, the geometry of which is predominantly favorable. This flexibility of the protein backbone at residue H151 of trypsin can be further quantitated by examining its relative movement in the four structures. The main chain atoms of Tn 150 through Tn 152 in the metal-bound structures move as much as 1 Å with respect to their positions in the apo structure. In contrast, His 143 of trypsin is more rigid, showing movement on the order of 0.3 Å between apo and metal-bound structures. The movement of His 151, reflected in its elevated *B*-factors, allowed this residue to achieve the greatest degree of planarity between its imidazole ring and the metal ions. The movement of main chain atoms could not be considered in modeling experiments described in the accompanying paper, although it does account, it part, for the deviation between the predicted and observed metal binding results.

The question exists whether or not the observed orientations and binding to metal are unduly influenced by metal ions being introduced into the already formed apo crystals *via* soaking instead of *a priori*, in solution, before any ordering or packing forces take place as part of the crystallization process. While the direct comparison of soaked *vs* cocrystallized metal structures cannot be made since cocrystallization of $Tn^{‡}E^{†}$ with metal was unsuccessful, the knowledge that the site was designed at the ends of a flexible surface loop that is highly accessible to solvent suggests that the critical residues can presumably move as necessary to accommodate the influx of metal as readily in the crystalline state as in solution. Furthermore, none of the engineered histidines are involved in any critical crystal packing contacts. This suggests that cocrystallization, had it been possible, would have resulted in a scenario similar to that observed in these soaked crystals.

The geometry of the metal binding site is dependent upon which metal is bound and seems to be dictated more by preferred geometry of the metal ion than the structural constraints of the protein as evidenced by the four distinct local environments adopted by both trypsin and ecotin in these structures. This observation is consistent with the fact that the site was designed at the ends of a flexible surface loop in trypsin where it is conceivable for movements to occur without a significant energetic barrier. It is the very flexibility of the loop regions that facilitates the accommodating movements of Tn N143H, E151H to enable metal binding. When the segment of trypsin from residue 139 to residue 154 in the apo $Tn^{‡}E^{†}$ structure is examined and compared with the same residues in the three metal-bound structures, a critical feature of the designed system is illustrated. All the main chain atoms of trypsin in each $Tn^{‡}E^{†}$ metal structure were superimposed upon those of the apo structure, excluding the main chain atoms in the immediate vicinity of the engineered site. The root mean square deviations of the positions of the patches of residues at the ends of the loop region were calculated. The deviations for the loop region as compared to the apo structure are substantial: zinc, copper, and nickel are 1.49, 1.33, and 1.61 Å, respectively. The copper and nickel structures show much greater similarity, as do the nickel and zinc structures with deviations of only 0.74 and 0.86 Å. When the same comparison is made between $Tn^{‡}E^{†}Zn$ and $Tn^{‡}E^{†}Cu$, a larger, 1.1 Å difference is observed. In effect, the zinc- and copper-bound cases are two extremes, with the nickel midway between the two.

The engineered tridentate pocket can be described as a geometry-driven binding site. When site-directed mutagenesis was used to add a second histidine to trypsin in order to enhance the interaction between the transition metal and the side chain of His 57, the strengths of the associations were found to be Cu^{2+} (21 μM) > Ni^{2+} (49 μM) > Zn^{2+} (128 μM) (Higaki et al., 1990). This is the order of association for the three metals for free imidazole in solution. The kinetics described in the accompanying paper, however, suggest that catalytic function follows the *opposite* trend, with the zinc-bound case showing the most functional arrangement and copper showing no turnover. Zinc commonly prefers a tetrahedral arrangement of ligands, the potential for which was designed into the binding site. This is one possible explanation for the significant increase in functional catalysis in the presence of zinc. For further understanding of the apparent contradiction between "chemical" affinity and the catalysis reported, the details of the structural features found in the crystal structures must be examined.

While there are easy to discern differences in the local geometries of the metal binding sites, a comparison of the entire complex of molecules reveals global similarity. When the different metal-bound $Tn^{‡}E^{†}$ complex molecules are superimposed on the apo complex, the rms deviations calculated (based on main chain atoms) range from a low of 0.38 Å for the copper and a high of 0.44 Å for the zinc comparison. If the main chain atoms of only the trypsins are superimposed and the rms deviations are again calculated for the whole $Tn^{‡}E^{†}$ complex, the copper-bound structure is again the most similar to the apo (rms deviation = 0.32 Å) while the zinc-bound structure is the most different (rms deviation = 0.43 Å). In both sets of calculations, the nickel- and copper-bound structures most closely resembled each other. This is interesting when viewed in the context of the level of stability of the anchoring of substrate in each structure. The apo and the zinc-bound structures represent the two extreme ends of the spectrum of this experiment, *i.e.*, the case in which the engineered histidine residues are not in position to bind metal and therefore no enhancement for the binding of substrate is expected, and the case thought to have the most noticeable positive effect on turnover, based on a metal binding geometry that achieves the closest adherence to planarity. In contrast, the nickel- and copper-bound structures do not achieve as favorable a geometry around their metal center, although they do indeed bind. Again, these two structures are reflective of the points between the extremes of the apo and zinc-bound structures.

How do these observed metal binding geometries compare to naturally occurring metal binding sites? There are several shapes available for the arrangement of anions about a metal cation. For example, if there are four coordinating ligands, their arrangement such that steric and repulsive interactions between them are minimized results in either a tetrahedral (angles of roughly 109.5°) or square-planar (angles of 90°) coordination polyhedra (Glusker, 1991). Likewise, if there are five coordinating ligands, the arrangement is usually square pyramidal (angles of 90°) or trigonal bipyramidal (angles of 60° and 90°). The possibility of distortion of these geometries exists, particularly in the case of Cu^{2+} metal centers, due to Jahn−Teller effects. Because the Cu^{2+} cation, with a d^9 electron configuration, contains an unpaired electron which can occupy either the (degenerate) $d_{x^2-y^2}$ or the d_{z^2} orbital, its ligand spheres may adopt a lower symmetry state in order to reduce the degeneracy. The observed manifestations of this distortion can be nonequivalent bond lengths for ligands about a metal center and even coordination in a different polyhedral scheme.

If the Cambridge Structural Database (Allen et al., 1979) is surveyed for high-quality (crystallographic $R < 10\%$) small molecule organometallic structures that mimic the binding of metal to histidyl imidazole groups, the following average metal to Nϵ2 bond lengths are observed. On the basis of 34 four-coordinate Zn^{2+} to imidazole ring bond lengths, the average observed bond length is 2.00(6) ± 0.01(7) Å. All of the organozinc compounds taken from the CSD were roughly tetrahedral. Similarly for Ni^{2+}, the average bond length is 2.10(2) ± 0.05(9) Å and 1.99(5) ± 0.02(2) Å for Cu^{2+}, based on 82 and 78 measured lengths, respectively. It should be noted that greater than 90% of the organonickel compounds used in the calculation of average bond length were six-coordinate and therefore a comparison of their ligand geometry to that found in $Tn^{‡}E^{†}$ is not meaningful. All the Cu^{2+} small molecule compounds included in the average bond length calculation were four-coordinate and represented a mixture of coordination polyhedra. On average, the bond lengths observed in the zinc-bound structure described in this paper are longer than the average small molecule value. The same is true for the nickel-bound structure, while no one trend exists for the copper-bound structure.

In naturally occurring proteins, the most common coordination number for zinc ions is 4, where the zinc ion is typically surrounded by a tetrahedral or distorted tetrahedral arrangement of ligands (Christianson, 1991). A prime example of this coordination geometry is found in the X-ray structure of wild-type human carbonic anhydrase II (Alexander et al., 1991). In this structure, Zn^{2+} is bound to three histidine residues and one solvent water molecule. The zinc−ligand bond lengths to histidines 94, 96, and 119 are 2.32, 2.45, and 2.28 Å, respectively, and the zinc−water bond length is 2.79 Å. The metal−histidine bond lengths are, on average, slightly longer than those observed in the structure of $Tn^{‡}E^{†}Zn$. The coordination polyhedral angles about the metal center in the carbonic anhydrase II structure are nearly polyhedral, with values of 107.7, 114.8, 102.9, and 104.2°. This bonding scheme is shown roughly superimposed upon the $Tn^{‡}E^{†}Zn$ metal binding site in Figure 6. The most notable differences between the naturally occurring carbonic anhydrase site and the site in $Tn^{‡}E^{†}Zn$ are the water molecule occupying the fourth coordination site and that a bond is formed to the Nδ1 of H119, as opposed to the Nϵ2 of Ec H86.

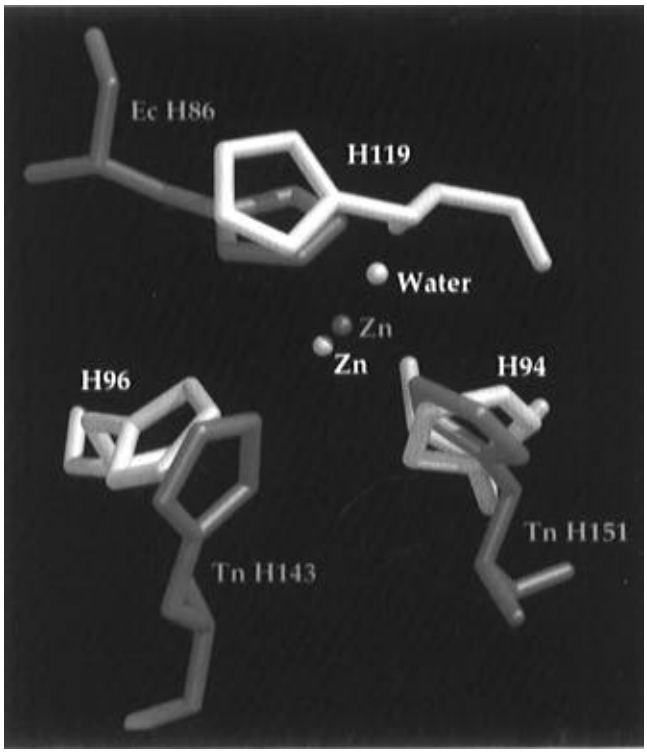

FIGURE 6: Superposition of the zinc binding site of carbonic anhydrase II (Alexander et al., 1991) on the zinc binding site of $Tn^{‡}E^{†}Zn$. Figure prepared with MidasPlus.

The geometry of the engineered metal binding site is dependent upon the metal that is bound. That the geometry is dictated by the preferred geometry of the specific metal ion instead of the structural constraints of the surrounding protein is key to the design of a metal binding site. The engineering of the site described in this study made use of the ends of a flexible surface loop in trypsin, where it is possible for movements to occur without overcoming a significant energetic barrier. It is the very flexibility of the loop regions that facilitates the accommodating movements of His 143 and His 151 of trypsin to enable metal binding and the subsequent anchoring of the substrate at His 86 of ecotin.

The introduction of all three metals perturbs the interactions between trypsin and ecotin. The details of these observed perturbations are critical to the understanding of why catalytic function in the $Tn^{‡}E^{†}$ system, in contrast to the affinity of these metals for free histidine in solution, follows the trend of zinc-bound being most functional, followed by nickel-bound, while copper-bound has no enzymatic turnover. The smaller movements made in the case of $Tn^{‡}E^{†}Zn$ incur the smallest detriment of catalytic register. Although other factors such as product release, conformational changes, and alternate potential weak binding sites may complicate the interpretation, these ground state structures provide useful information for subsequent design.

Finally, two additional conclusions can be drawn from a comparison of the results of the modeling experiments described in the accompanying paper and the structural results discussed here. First, modeling experiments should take into consideration that main chain movements can occur to accommodate metal binding. While the movements of side chains could be adequately modeled, the X-ray crystal

structures clearly demonstrate that a combination of main chain shifts and side chain movements allowed for complexation with metal. Second, it is interesting to note that naturally occurring metalloprotein binding sites have geometries that more closely resemble the geometries found for metal-containing small molecules. Many iterations of mutations and other alterations have taken place in the natural evolution of metalloproteins, factors that are not easily simulated by modeling calculations. The engineered site described here did achieve effective binding to zinc, copper, and nickel, despite their deviations from theoretically optimal binding geometries.

ACKNOWLEDGMENT

We thank Mary E. McGrath for making available the starting set of copper parameters and also Thomas J. Stout for technical advice and critical reading of the manuscript.

REFERENCES

Adman, E. T., & Jenson, L. H. (1981) *Isr. J. Chem. 21*, 8−12.
Adman, E. T., Stenkamp, R. E., Sieker, L. C., & Jensen, L. H. (1978) *J. Mol. Biol. 123*, 35−47.
Alexander, R. S., Nair, S. K., & Christianson, D. W. (1991) *Biochemistry 30*, 11064−11072.
Allen, F. H., Bellard, S., Brice, M. D., Cartwright, B. A., Higgs, H., Hummelink, T., Hummelink-Peters, B. G., Kennard, O., Motherwell, W. D. S., Rodgers, J. R., & Watson, D. G. (1979) *Acta Crystallogr., Sect. B 35*, 2331−2339.
Bernstein, F. C., *et al.* (1977) *J. Mol. Biol. 112*, 535−542.
Browner, M. F., Fauman, E. B., & Fletterick, R. J. (1992) *Biochemistry 31*, 11297−11304.
Browner, M. F., Hackos, D., & Fletterick, R. (1994) *Struct. Biol. 1*, 327−333.
Brunger, A. T., Kuriyan, J., & Karplus, M. (1987) *Science 235*, 458−460.
Chakrabarti, P. (1990) *Protein Eng. 4*, 57−63.
Chambers, J. L., Cristoph, G. G., Krieger, M., Kay, L., & Stroud, R. M. (1974) *Biochem. Biophys. Res. Commun. 59*, 70−74.
Christianson, D. W. (1991) *Adv. Protein Chem. 42*, 281−355.
Fuh, G., & Wells, J. A. (1995) *J. Biol. Chem. 270*, 13133−13137.
Glusker, J. P. (1991) *Adv. Protein Chem. 42*, 1−75.
Guss, J. M., & Freeman, H. C. (1983) *J. Mol. Biol. 169*, 521−563.
Guss, J. M., Harrowell, P. R., Murata, M., Norris, V. A., & Freeman, H. C. (1986) *J. Mol. Biol. 192*, 361−387.
Hakansson, K., Carlsson, M., Svensson, L. A., & Liljas, A. (1992) *J. Mol. Biol. 227*, 1192−1204.
Halfon, S., & Craik, C. S. (1996) *J. Am. Chem. Soc*. (in press).
Hall, T. M. T., Porter, J. A., Beachy, P. A., & Leahy, D. J. (1995) *Nature 378*, 212−216.
He, G. P., Muise, A., Li, A. W., & Ro, H. S. (1995) *Nature 378*, 92−96.
Higaki, J. N., Haymore, B. L., Chen, S., Fletterick, R. J., & Craik, C. S. (1990) *Biochemistry 29*, 8582−8586.
Ibers, J. A., & Holm, R. H. (1980) *Science 209*, 223−235.
Ippolito, J. A., & Christianson, D. W. (1994) *Biochemistry 33*, 15241−15249.
Jabri, E., Carr, M. B., Hausinger, R. P., & Karplus, P. A. (1995) *Science 268*, 998−1004.
Lesburg, C. A., & Christianson, D. W. (1995) *J. Am. Chem. Soc. 117*, 6838−6844.
Martell, A. D., & Smith, R. M. (1974) *Critical Stability Constants*, Plenum Press, New York.
McGrath, M. E., Haymore, B. L., Summers, N. L., Craik, C. S., & Fletterick, R. J. (1993) *Biochemistry 32*, 1914−1919.
McGrath, M. E., Erpel, T., Bystroff, C., & Fletterick, R. J. (1994) *EMBO J. 13*, 1502−1507.
McPherson, A. (1989) *Preparation and Analysis of Protein Crystals*, Robert E. Kreiger Publishing Co., Malabar, FL.
Navaza, J. (1994) *Acta Crystallogr. A 50*, 157−163.
Norris, G. E., Anderson, B. F., & Baker, E. N. (1983) *J. Mol. Biol. 165*, 501−521.
Norris, G. E., Anderson, B. F., & Baker, E. N. (1986) *J. Am. Chem. Soc. 108*, 2784−2785.
Otwinowski, Z. (1990) *HKL*, Yale University, New Haven, CT.
Ponder, J. W., & Richards, F. M. (1987) *J. Mol. Biol. 193*, 775−791.
Quiocho, F. A., & Lipscomb, W. N. (1971) *Adv. Protein Chem. 25*, 1−78.
Rees, D. C., Lewis, M., & Lipscomb, W. N. (1983) *J. Mol. Biol. 168*, 367−387.
Regan, L. (1995) *Trends Biochem. Sci. 20*, 280−285.
Roberts, V. A., Iverson, B. L., Iverson, S. A., Benkovic, S. J., Lerner, R. A., Getzoff, E., D., & Tainer, J. A. (1990) *Proc. Natl. Acad. Sci. U.S.A. 87*, 6654−6658.
Sack, J. S. (1988) *J. Mol. Graphics 6*, 224−225.
Schneider, G., Eklund, H., & Cetergren-Zeppezauer, M. (1983) *Proc. Natl. Acad. Sci. U.S.A. 80*, 5289−5293.
Somers, W., Ultsc, M., De Vos, A. M., & Kossiakoff, A. A. (1994) *Nature 372*, 478−481.
Willett, W. S., Gillmor, S., Perona, J. J., Fletterick, R. J., & Craik, C. S. (1995) *Biochemistry 34*, 2172−2180.
Willett, W. S., Brinen, L. S., Fletterick, R. J., & Craik, C. S. (1996) *Biochemistry 35*, 5992−5998.
Yagami-Hiromasa, T., Sato, T., Kurisaki, T., Kamijo, K., Nabeshima, Y., & Fujisaww-Sehara, A. (1995) *Nature 377*, 652−656.

BI9530200